Temperature compensation of silicon Lamé resonators using etch holes: theory and design methodology

Luca Luschi, Giuseppe Iannaccone, *Fellow, IEEE*, and Francesco Pieri

***Abstract*—We present a new approach to the temperature compensation of MEMS Lamé resonators, based on the combined effect of the doping concentration and of the geometry of etch holes on the equivalent temperature coefficients of silicon. To this purpose, we develop and validate an analytical model which describes the effect of etch holes on the temperature stability of Lamé resonators through comparison with experiments available in the literature and FEM simulations. We show that two interesting regions of the design space for Lamé resonators exist, where a cancellation of the first-order temperature coefficient of the resonance frequency is possible: [100]-oriented silicon with n-doping of 2.5·10^{19} cm^{-3}, and [110]-oriented silicon with p-doping higher than 1.4·10^{20} cm^{-3}.**

***Index Terms*— Microelectromechanical systems, Resonators, Micromachining, Doping, Temperature dependence.**

I. INTRODUCTION

The potential use of MEMS resonators in a wide range of applications, including frequency control, RF filters and oscillators [1], [2], as well as chemical and biochemical sensing [3]–[6], has been proposed and intensely investigated in the last two decades, with some of these devices finally reaching the market [7].

A critical aspect of MEMS resonators, especially in the case of frequency control applications, is their temperature stability: if not properly compensated, the temperature coefficient of MEMS resonators can be in the order of tens of ppm·K^{-1}, orders of magnitude larger than that of quartz resonators [1], [8]. For the most demanding applications, a temperature stability of only a few (or even fractions of) ppm over the whole temperature range is required [9]. Although with less strict constraints, temperature stability is also a concern for resonant sensing applications [4], [10]. For the most part, the large temperature drift of silicon resonators can be attributed to the strong temperature dependence of its elastic constants.

Several active and passive temperature compensation techniques have been developed. Active techniques exploit a temperature sensor together with a continuous control of a parameter of the resonator/oscillator system. By reading the resonator temperature and subsequently adjusting this parameter, the temperature drift of the resonance frequency can be compensated. A possible choice of the control parameter is the temperature of the resonator itself, thus realizing the so-called ovenized configuration [11]–[14]. Other possible choices are the DC bias voltage of a capacitively actuated resonator [15], or a temperature-controlled frequency synthesizer cascading the oscillator [16]. Passive compensation techniques rely on changing the resonator properties at the time of fabrication by introducing a properly chosen second material. The temperature drift of silicon elastic moduli can be compensated by including silicon oxide in the resonator body [17], [18]. The different thermal expansion coefficient of nickel [19], [20] or silicon carbide [21] with respect silicon has been exploited in order to induce thermal stresses in the resonator.

Active compensation techniques are typically more effective in achieving temperature stability than passive compensation techniques, at the price of higher power consumption and larger area occupation. Passive compensation techniques typically require ad-hoc steps in the fabrication technology. In order to reach quartz-like performances, multiple compensation techniques have to be employed simultaneously [11], [13], [14], [16]. Recently, a passive compensation technique based on doped resonators made of Single-Crystal Silicon (SCS) has raised much attention [8], [22]–[25]. Doping modifies the carrier contribution to the elastic constants, which are the main source of temperature instability of SCS [26]. Doping of SCS is a well-developed technology that can be introduced without a significant increase in cost and complexity.

In some of the works cited above [22], [24], the temperature coefficients of resonators with small release etch holes have also been measured. These measurements show that the temperature coefficient may be affected by the presence of holes, depending on doping concentration, resonance mode and orientation. This effect is captured by brute-force FEM analysis, but a simple theoretical model is lacking.

Among the possible types of MEMS resonators, Lamé resonators have been extensively investigated [6], [14], [27], [28]. They ideally have a vibration mode exhibiting pure shear deformation (i.e. with no local change in volume), a fact that

This work was supported in part by the ENIAC Joint Undertaking under Grant 325622.

The authors are with the Dipartimento di Ingegneria dell'Informazione, Università di Pisa, Pisa, 56122 Italy (e-mail: luca.luschi@for.unipi.it, {f.pieri, g.iannaccone}@iet.unipi.it).

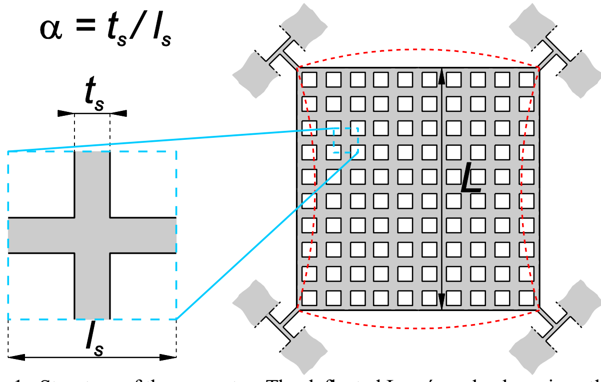

Fig. 1. Structure of the resonator. The deflected Lamé mode-shape is outlined in red. The geometry of the unit cell of the holes pattern, along with its dimensions, is shown in the inset.

has been linked to very low thermoelastic losses, and thus very high quality factors when the materials losses are prevalent (i.e. at very low pressure) [29].

In this work, we propose a new approach to the temperature compensation of silicon Lamé resonators based on the combined effect of doping concentration and etch holes geometry. For thin resonators, we give a simple analytical method which predicts the effect of etch holes on the temperature stability and can be used to design resonators with nominal zero first-order temperature coefficient. Etch holes are often required in MEMS devices for release purposes, but may also be introduced to increase the sensitivity of resonant sensors, by increasing their surface to volume ratio [30], [31].

By using the data presented in [22], [23], we also investigate the relation between temperature coefficient and doping in perforated resonators. We show that a better insight on these effects can be obtained by describing SCS elasticity through its elastic moduli E, G and ν (i.e. its Young's modulus, shear modulus, and Poisson's ratio) rather than with its elastic constants C_{11}, C_{12}, C_{44}, as it is done in [22], [23]. This alternative description can be computed from the data presented in the cited works through a simple transformation of variables (see Appendix A for details). We validate the model with available experiments and FEM simulations. Our method can be very effective even if doping concentration is experimentally affected by significant inaccuracy, because it can be used in regions of the design space in which the sensitivity of the temperature coefficient of the resonance frequency to doping is strongly suppressed.

II. Model Derivation

A model for the temperature coefficient of thin perforated Lamé resonators can be derived from the resonance frequency model already presented in [32], where holes are taken into account through a cellular material approach [33]. For the purpose of this work, cellular materials are microstructured solids obtained by periodic repetition of a unit cell. The structure of the resonator is given in Fig. 1. In the course of this paper, we denote as "full" a resonator without holes. The Lamé resonance frequency of a full resonator has an exact closed form expression:

$$f_0 = \frac{1}{L}\sqrt{\frac{G_d}{2\rho}} \quad (1)$$

where L is the length of the resonator side, ρ is the mass density and G_d is the shear modulus along a direction parallel to a diagonal of the square. Remarkably, even for anisotropic materials, there are two directions (separated by 45°) for which (1) is also valid [34]. In the case of SCS, which has a cubic symmetry, these two directions are [100] and [110], and Lamé modes are sustained only for resonators with sides aligned along these directions. In a material with cubic symmetry the diagonal shear moduli for these directions are $(C_{11}\text{-}C_{12})/2$ and C_{44}, respectively [35]. In both these directions, the shear modulus along the diagonal can be expressed as a function of E_p and ν_p, which are the Young's modulus and Poisson's ratio computed along a direction parallel to the resonator side:

$$G_d = \frac{E_p}{2(1+\nu_p)} \quad (2a)$$

or, more specifically,

$$G_{[110]} = \frac{C_{11}-C_{12}}{2} = \frac{E_{[100]}}{2(1+\nu_{[100]})},\ G_{[100]} = C_{44} = \frac{E_{[110]}}{2(1+\nu_{[110]})} \quad (2b)$$

(see Appendix A for details). While (1) and (2) are strictly valid for full resonators only, they can be generalized to resonators with holes if we assume that the hole pitch (l_s) is small compared to the resonator side L. If this is the case, the perforated resonator can be modeled with effective parameters substituted into the expression for the resonant frequency of the full Lamé resonator:

$$f_{0,eq} = \frac{1}{L}\sqrt{\frac{G_{d,eq}}{2\rho_{eq}}} = \frac{1}{L}\sqrt{\frac{E_{p,eq}}{4(1+\nu_{p,eq})\rho_{eq}}} \quad (3)$$

where $E_{p,eq}$ and $\nu_{p,eq}$ are the equivalent Young's modulus and Poisson's ratio along directions parallel to the sides of the resonator and ρ_{eq} is the equivalent mass density. This corresponds to a description of the perforated material as an equivalent material with specific effective elastic constants. This description holds true if the perforated material retains cubic symmetry in the plane, i.e. both the hole geometry and the underlying crystal structure are invariant by 90° rotation and reflection along two orthogonal axes. Square lattices of square or circular holes aligned along the [100] or [110] directions of a cubic crystal have this symmetry. These types of grids comprise most MEMS designs.

Accurate expressions for $E_{p,eq}$, $\nu_{p,eq}$ and ρ_{eq} are given in [32] as a function of the fill factor α, i.e. the ratio of the distance between holes t_s to the pitch l_s (Fig. 1), and of a fitting parameter k, which depends only on the SCS orientation, but not on the doping or temperature:

$$\begin{cases} E_{p,eq} = & \alpha\frac{1+(1-\alpha)\alpha^{k-1}}{1+\alpha^{k-1}(1-\alpha)^2}E_p \\ \nu_{p,eq} = & \alpha\frac{1+(1-\alpha)\alpha^{k-1}}{1+\alpha^{k-1}(1-\alpha)^2}\nu_p \\ \rho_{eq} = & \alpha(2-\alpha)\rho \end{cases} \quad (4)$$

where E_p, ν_p are the SCS Young's modulus and Poisson's ratio along directions parallel to the sides of the resonator, respectively, and ρ is the SCS density. The used optimum

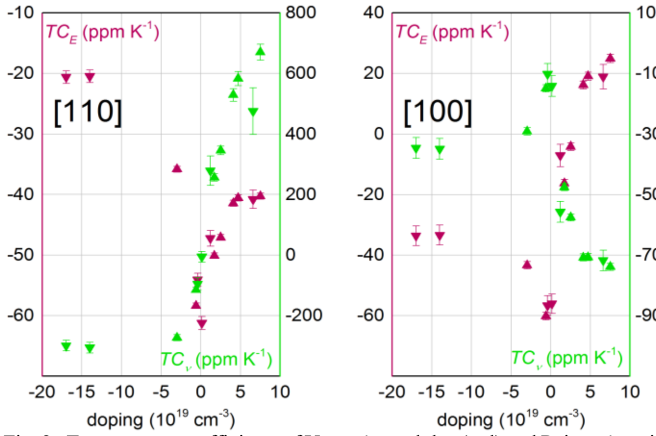

Fig. 2. Temperature coefficients of Young's modulus (red) and Poisson's ratio (green) along [110] (left) and [100] (right) directions as a function of the doping concentration. Down corner triangles are based on data from [22], up corner triangles on data from [23].

values of k were determined using the approach in [32] and were 2.85 for [100] SCS (all dopings and temperatures), 3.45 for [110] SCS (all dopings and temperatures).

These expressions were obtained assuming a plane stress hypothesis in the unit cell. Substituting these expressions into (3) gives the resonance frequency of a square-perforated Lamé resonator:

$$f_{0,eq} = \frac{1}{L}\sqrt{\frac{E_p[1+(1-\alpha)\alpha^{k-1}]}{4(2-\alpha)\rho\left[1+\alpha^{k-1}(1-\alpha)^2+\alpha\left(1+\alpha^{k-1}(1-\alpha)\right)\nu_p\right]}}. \quad (5)$$

By taking the derivative of (5) with respect to the temperature, the expression for the linear temperature coefficient of square perforated Lamé resonators can be found. In differentiating (5), we make use of the fact that α is not a function of temperature, as both l_s and t_s are changed in the same way and their ratio is thus constant. The result of this differentiation is:

$$TC_f = \frac{1}{f_{0,eq}}\frac{\partial f_{0,eq}}{\partial T} =$$

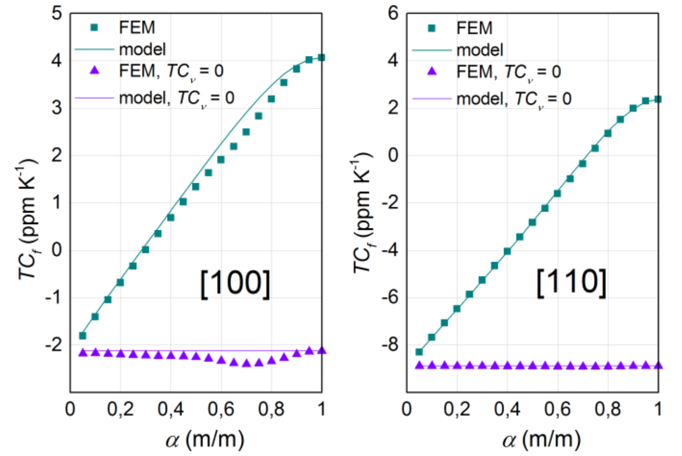

Fig. 3. Frequency temperature coefficients of [100] (left) and [110] (right) Lamé resonators as a function of the fill factor α: comparison between FEM simulations and model predictions. The elastic constants are the ones labelled As1.2 (for [100]) and B17 (for [110]) in Table 1. The value of k used for the model is 2.85 for the [100] graph, and 3.45 for the [110] graph.

$$= -TC_L + \frac{1}{2}TC_{Ep} - \frac{1}{2}TC_\rho - \frac{1}{2}\frac{[\alpha+\alpha^k(1-\alpha)]\nu_p}{1+\alpha^{k-1}(1-\alpha)^2+[\alpha+\alpha^k(1-\alpha)]\nu_p}TC_{\nu p} \quad (6)$$

where TC_x denotes the temperature coefficient of quantity x. It is straightforward that $TC_\rho = -3TC_L$, so that (6) can be further simplified to:

$$TC_f = \frac{1}{2}TC_L + \frac{1}{2}TC_{Ep} - \frac{1}{2}\frac{[\alpha+\alpha^k(1-\alpha)]\nu_p}{1+\alpha^{k-1}(1-\alpha)^2+[\alpha+\alpha^k(1-\alpha)]\nu_p}TC_{\nu p}. \quad (7)$$

We note here that (5)-(7) are only valid for $\alpha > 0$. On the right-hand side of (7) we can identify the following terms, in order: the contribution of the thermal expansion of silicon, the contribution of its Young's modulus and finally the contribution of its Poisson's ratio. The first two terms are identical to the ones found in the expression for the TC_f of a resonator with no holes. The last one, on the contrary, is affected by the presence of holes (through α). Its contribution

TABLE I
COMPUTED ELASTIC CONSTANTS E AND N FOR SILICON AND THEIR TEMPERATURE COEFFICIENTS ALONG [100] AND [110] DIRECTIONS. P-TYPE DOPING VALUES ARE REPORTED WITH A NEGATIVE SIGN.

Reference	Doping (cm^{-3})	$E_{[100]}$ (GPa)	$TC_{E[100]}\cdot10^6$ (K^{-1})	$\nu_{[100]}$ (-)	$TC_{\nu[100]}\cdot10^6$ (K^{-1})	$E_{[110]}$ (GPa)	$TC_{E[110]}\cdot10^6$ (K^{-1})	$\nu_{[110]}$ (-)	$TC_{\nu[110]}\cdot10^6$ (K^{-1})
[22] B17	-1.7·10^{20}	127.6±1.1	-33.6±3.3	0.280±2.4·10^{-3}	-34.6±3.4	162.9±0.5	-20.6±1	(8.14±0.34)·10^{-2}	-299.1±17.4
[22] B14	-1.4·10^{20}	127.5±1.1	-33.4±3.3	0.281±2.4·10^{-3}	-34.9±3.4	163.1±0.5	-20.5±1	(8.00±0.34)·10^{-2}	-306.0±17.9
[22] B0.4	-4.1·10^{18}	129.6±2.3	-56.6±3.2	0.280±4.1·10^{-3}	-10.1±3.4	168.5±1.3	-54.1±1.1	(6.38±0.77)·10^{-2}	-95.9±20.4
[22] Sb0.1	1.3·10^{18}	129.5±2.3	-56.1±3.2	0.280±4.1·10^{-3}	-14.1±3.4	168.6±1.3	-61.2±1.1	(6.30±0.77)·10^{-2}	-5.56±17.8
[22] As1.2	1.2·10^{19}	126.7±2.4	-7.1±3.7	0.285±4.1·10^{-3}	-55.7±3.4	166.7±1.3	-47.2±1.3	(6.03±0.79)·10^{-2}	278.7±48.7
[22] P6.6	6.6·10^{19}	125.4±2.4	18.9±4.1	0.289±4.1·10^{-3}	-71.8±3.4	165.8±1.3	-40.8±1.5	(6.02±0.80)·10^{-2}	475.9±77.1
[23] B0.6	-6·10^{18}	130.1±0.4	-60.2±1.2	0.2779±4.8·10^{-4}	-14.9±1.2	169.0±0.3	-58.4±0.5	(6.18±0.17)·10^{-2}	-114.9±8.3
[23] B3	-3·10^{19}	128.8±0.4	-43.4±1.3	0.2789±4.9·10^{-4}	-29.1±1.2	167.1±0.3	-35.8±0.5	(6.43±0.17)·10^{-2}	-273.6±10.2
[23] As1.7	1.7·10^{19}	127.8±0.4	-16.3±1.3	0.2816±4.9·10^{-4}	-47.6±1.2	167.9±0.3	-50.1±0.5	(5.60±0.17)·10^{-2}	256.1±12.1
[23] As2.5	2.5·10^{19}	127.0±0.4	-4.2±1.3	0.2838±4.9·10^{-4}	-57.6±1.2	167.5±0.3	-47.1±0.5	(5.50±0.17)·10^{-2}	345.7±14.6
[23] P4.1	4.1·10^{19}	125.5±0.4	16.2±1.3	0.2863±4.9·10^{-4}	-70.8±1.2	166.7±0.3	-41.5±0.5	(5.24±0.17)·10^{-2}	529.1±20.8
[23] P4.7	4.7·10^{19}	124.7±0.4	19.1±1.3	0.2879±4.9·10^{-4}	-70.7±1.2	166.2±0.3	-40.6±0.5	(5.06±0.17)·10^{-2}	583.1±23.3
[23] P7.5	7.5·10^{19}	123.0±0.4	24.9±1.4	0.2905±4.9·10^{-4}	-73.9±1.2	164.8±0.3	-40.3±0.5	(4.95±0.17)·10^{-2}	670.4±27

to the total TC_f goes from its (absolute) maximum for a full resonator ($\alpha = 1$), down to very small values for smaller and smaller α's. Its expression suggests that the total TC_f can be tuned (i.e. reduced or even cancelled) by a careful choice of α.

Actual values of TC_f for SCS resonators given by (7) cannot be obtained without taking into account that ν_p, and even more TC_{Ep} and $TC_{\nu p}$, depend on the doping concentration. Therefore, these dependencies have to be made explicit. To this purpose, we use the extensive experimental characterization of the temperature dependence of the stiffness coefficients C_{11}, C_{12} and C_{44} of SCS presented in [22], [23].

The calculated values for the TC_{Ep} and $TC_{\nu p}$ are reported in Table I for each doping for which experimental data are available [22], [23]. These values will be used, together with (7), to estimate the TC_f of perforated Lamé resonators.

We remark that doping strongly affects the temperature coefficients of both the Young's modulus and Poisson's ratio, while leaving their respective values (computed at the reference temperature of 25°C) almost unchanged with respect to the undoped case. As a consequence, from the point of view of the effect of holes on the temperature stability of the resonance frequency, the most important quantities are TC_{Ep} and $TC_{\nu p}$. For this reason, we plot in Fig. 2 their values as a function of the doping concentration, for the [100] and [110] directions, respectively. To retain consistency with the graphs reported in [22], [23], the data for p-type doping are reported on the negative side of the x axis.

III. Validation

A. FEM

We use the values reported in Table I together with (7) for the estimation of the TC_f of perforated Lamé resonators. To validate the model over the range [0.05, 1] of α, we present a comparison between model predictions and FEM (Finite-Elements Method) simulations.

We have performed FEM simulations with ANSYS of two Lamé resonators with sides aligned along [100] and [110] directions. We have defined SCS through its three independent elastic constants along [100], namely $E_{[100]}$, $\nu_{p[100]}$ and $G_{[100]} = C_{44}$. The first two appear in Table I, and the latter was taken directly from references [22], [23]. A density of 2330 kg·m^{-3} and a coefficient of linear thermal expansion TC_L of 2.84 ppm·K^{-1} were used. The values of the p-type doping named B17 have been used for the [110] resonator, while those of the n-type doping As1.2 have been used for the [100] resonator. A side length of 400 μm and 30 square holes along the side have been used for all the simulated resonators. To check for a possible effect of the number of holes on the results, simulations were also carried out with 20 and 40 holes along the side, and the difference of the associated results with the 30-hole case were negligible. In the following, only the result for the 30-hole case are reported. The fill factor α varies in the range 0.05,1 in steps of 0.05. For each of these geometries, the temperature have been swept in the range -40, 85°C with steps of 5°C. All the simulations have been performed under a 2D plane-stress hypothesis and meshing the geometry with around 10^5 PLANE182 elements. By fitting the Lamé resonance frequencies obtained from the modal analysis with a second order polynomial, the linear temperature coefficients as a function of α have been obtained.

The plane-stress hypothesis is a reasonable assumption at least for thin resonators and for small holes, being the full Lamé case a problem with zero out-of-plane deformations (i.e. a problem where plane-stress and plane-strain hypothesis yield the same results). Deviations from plane-stress results are expected in real (three dimensional) resonators with large holes and low length-to thickness-ratio. The effect of finite thickness will be discussed for a few important cases in section IV.

The results of FEM simulations are reported in Fig. 3 for a [100] n-doped resonator at $1.2\cdot10^{19}$ cm^{-3} (As1.2 of Table I) and for a [110] p-doped resonator at $1.7\cdot10^{20}$ cm^{-3} (B17 of Table I). The model reproduces very well the results of simulations over the whole α range. Small differences (typically smaller than 0.5 ppm·K^{-1}) can be observed in the [100] case. As stated in the comments to (7), the contribution of the Poisson's ratio to TC_f is the only term affected by α. The model thus suggests that a Lamé resonator made of a material having a temperature-independent ν_p will have a TC_f independent of α. In order to verify such property, we repeated the simulations using fictitious materials having the same properties as the ones reported in Table I, except for a constant Poisson's ratio ($TC_{\nu p} = 0$). The results (reported as triangles in Fig. 3) confirm the expected behavior: the holes affect the TC_f of the resonators essentially only through the change of the temperature behavior of the equivalent material Poisson's ratio. The properties of this material can be tailored by changing the geometry of the holes.

TABLE II
Comparison of experimentally measured and modeled temperature coefficients of perforated Lamé resonators

Reference	Doping (cm^{-3})	Orient.	TC_f (perforated resonator, $\cdot10^6$) (K^{-1})		TC_f (full resonator, $\cdot10^6$) (K^{-1})
			exp.	model	exp.
[22] B17	$-1.7\cdot10^{20}$	[100]	-11.99	-11.97 ± 1.93	-11.64
[22] B14	$-1.4\cdot10^{20}$	[100]	-11.84	-11.81 ± 1.94	-11.4
[22] B0.4	$-4.1\cdot10^{18}$	[100]	-25.91	-25.89 ± 1.92	-
[22] Sb0.1	$1.3\cdot10^{18}$	[100]	-25.46	-25.24 ± 1.92	-
[22] As1.2	$1.2\cdot10^{19}$	[100]	3.20	3.49 ± 2.15	-
[22] P6.6	$6.6\cdot10^{19}$	[100]	17.75	18.18 ± 2.32	-
[22] B17	$-1.7\cdot10^{20}$	[110]	0.86	1.03 ± 0.31	2.37
[22] B14	$-1.4\cdot10^{20}$	[110]	1.048	1.17 ± 0.31	2.55
[22] B0.4	$-4.1\cdot10^{18}$	[110]	-23.03	-23.08 ± 0.34	-
[22] Sb0.1	$1.3\cdot10^{18}$	[110]	-29.08	-29.05 ± 0.34	-
[22] As1.2	$1.2\cdot10^{19}$	[110]	-29.85	-29.17 ± 0.35	-
[22] P6.6	$6.6\cdot10^{19}$	[110]	-31.83	-30.84 ± 0.37	-
[23] P4.7	$4.7\cdot10^{19}$	[100]	18	18.43 ± 0.78	18.6
[23] P4.7	$4.7\cdot10^{19}$	[110]	-32	-31.88 ± 0.20	-32.7

B. Experimental

For validation with literature data, we preliminarily estimate the fill factors. The devices presented in [22] have small circular holes, 2 μm in diameter, arranged over a square matrix with a pitch of 10 μm [36]. For TC_f estimation of these devices, the circular holes have been approximated with square holes with side equal to the circle diameter, resulting in a fill factor $\alpha = 0.8$. The same approximation has been done for the n-type resonator presented in [24], where the hole diameter is 3 μm and the pitch

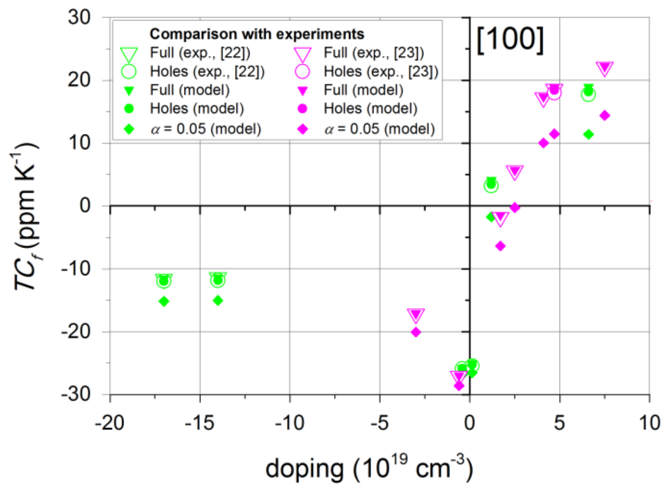

Fig. 4. Temperature coefficients of [100] Lamé resonators.

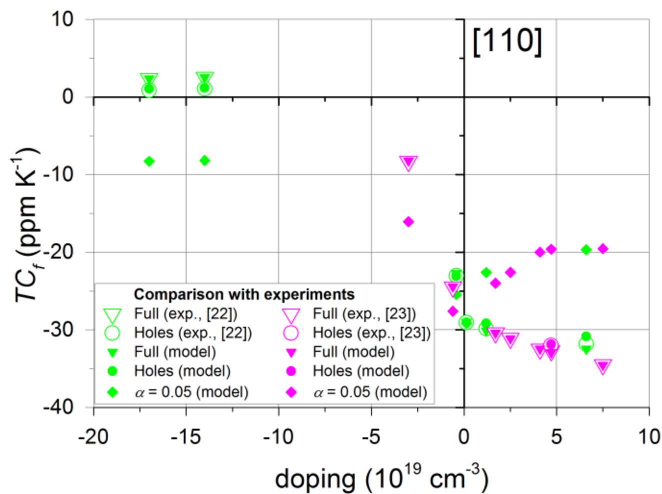

Fig. 5. Temperature coefficients of [110] Lamé resonators.

is 20 µm, resulting in $\alpha = 0.85$. For the exact doping concentration of the latter structure ($5\cdot10^{19}$ cm^{-3}), the stiffness constants and their temperature coefficients are not available in literature, thus we have used values from a slightly different doping concentration ($4.7\cdot10^{19}$ cm^{-3}) measured by the same authors [23], i.e. the one labelled as P4.7 in Table I.

The comparisons between the model predictions and the measured TC_f's are reported in Table II. As a consequence of the high values of α, the changes in TC_f between the full and perforated case are never larger than few ppm·K^{-1}.

IV. Discussion

The connection between the presence and dimensions of holes and the value of the TC_f, which is implied by (7), suggests that holes can be effectively used as a method to strongly suppress, or even cancel, the first-order dependence of the resonance frequency on the temperature. The design parameters for a zero-TC_f resonator are the resonator orientation ([100] or [110]), its doping value, and its fill factor α. For high-Q applications, a high value of α (i.e. small holes) is also desirable, as large holes are known to affect the quality factor unfavorably [37], [38]. The worsening of Q is not dealt with in this paper, but it is clearly important in applications. the observed Q lowering in vacuum is thought to be caused primarily by thermoelastic damping (TED), and typically impacts the Q value between one and two orders of magnitude with respect to full Lamé resonators, depending on the value of α [22], [37], [38]. Smaller α's give lower Q's, because the local rate of volume change during vibration (and associated TED losses) becomes larger as the holes get larger. The addition of holes can thus be considered as an additional degree of freedom that can be used to reach a compromise between Q and TC_f, with both parameters being important in applications.

The change in TC_f that can be obtained by introducing holes can be estimated by applying our model to all the possible doping concentrations presented in Table I. For each concentration, the extreme values of TC_f obtained for the full resonators ($\alpha = 1$) and for resonators close to hollow (i.e. for $\alpha = 0.05$) give a realistic tuning range of TC_f that can be covered by changing the hole size (at fixed pitch). These extreme values are represented as solid triangles and diamonds in Figs. 4 and 5 for the [100] and [110] directions, respectively. For doping values for which a measure of the TC_f is available in Table II, such value is also added to the graphs (using white symbols), along with its corresponding value provided by our model (solid symbols).

From inspection of Figures 4 and 5 it is clear that zero-TC_f full resonators (triangles) could be theoretically designed by tuning the doping concentration. For example, the TC_f for [100] resonators likely crosses zero at a donor concentration of around $2.5\cdot10^{19}$ cm^{-3}, while the same should occur for an acceptor concentration of around $1\cdot10^{20}$ cm^{-3} for [110] resonators. However, the practical chance of zeroing the TC_f through an appropriate choice of the doping concentration is undermined by the limited accuracy of the doping process. Typical doping tolerances are in the range of ±10% [39]. Such inaccuracy will have an impact on the temperature stability of the resonator that is proportional to the sensitivity of TC_f to doping concentration: the steeper the TC_f-doping characteristic is, the smaller the control of TC_f will be.

The presence of holes, by introducing another degree of freedom in the design, enables a different approach to zero-TC_f resonators. Examination of (7) suggests the TC_f can be cancelled only if the contributions of the Young's modulus and Poisson's ratio (i.e. the second and third term in the RHS of (7))

TABLE III
Fill factors that provide zero-TC_F resonators according to model and FEM.

Reference	Doping (cm^{-3})	Orientation	model	2D FEM (plane stress)	3D FEM (thickness = 10µm)	2D FEM (plane strain)	3D FEM (thickness = 40µm)
[22] B17	$-1.7\cdot10^{20}$	[110]	0.714	0.727	0.735	0.752	0.745
[22] B14	$-1.4\cdot10^{20}$	[110]	0.704	0.717	0.726	0.744	0.737
[22] As1.2	$1.2\cdot10^{19}$	[100]	0.283	0.299	0.401	0.545	0.529
[23] As2.5	$2.5\cdot10^{19}$	[100]	0.083	0.092	0.214	0.416	0.394

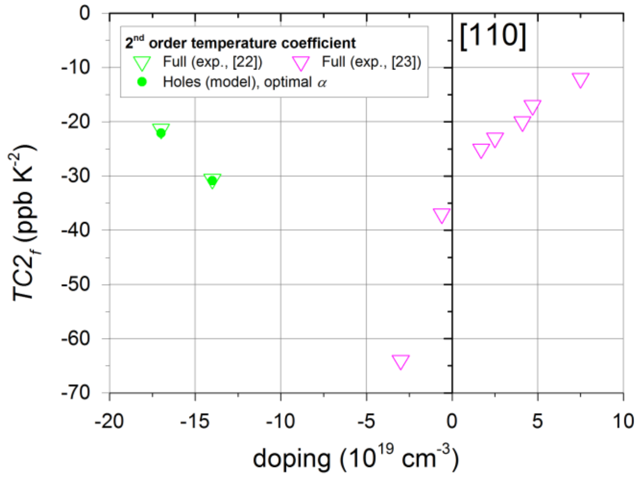

Fig. 6. Second order temperature coefficient $TC2_f$ of [110] Lamé resonators.

have the same sign and approximately the same absolute value, as the contribution of thermal expansion (i.e. the first term) is only 1.42 ppm·K^{-1}, and essentially unaffected by doping [40]. As the coefficient multiplying TC_{vp} in (7) is of the order of 0.1, the second and third term in (7) cancel out only if TC_{vp} is around 10 times larger than TC_{Ep}. This is not possible for undoped resonators, where TC_{vp} is typically comparable or even smaller than TC_{Ep}. The effect of the Young's modulus is thus dominant on the TC_f of undoped resonators, so that their TC_f's are close to ½TC_{Ep} (or around -30 ppm·K^{-1}).

However, the changes introduced by the doping on the temperature coefficients allow at least two different doping regions suited for the compensation. The first, for [100] resonators, can be identified by considering the plot in Fig. 2, where $TC_{E[100]}$ crosses zero for an n-type doping of around 2.5·10^{19} cm^{-3}, in a region where the corresponding $TC_{v[100]}$ is several tens of ppm·K^{-1}. The second, for [110] resonators, is in the highly doped (>1.4·10^{20} cm^{-3}) p-type region of the [110] plot in Fig. 2. In this second case, an order of magnitude between the temperature coefficients is reached due to the steep decrease of $TC_{v[110]}$, which is around -300 ppm·K^{-1}.

Data for the extreme values of TC_f presented in Figs. 4-5 show that these two doping windows are the only ones for which TC_f crosses zero by sweeping α between 1 (solid triangles) and 0 (solid diamonds). Computing the value α_{opt} leading to zero TC_f from (7) is straightforward, once the material properties are known. The results of this computation are reported in the "model" column of Table III. In order to evaluate 3D effects, we also added FEM estimates of α_{opt} for 2D plane-stress, 2D plane-strain and 3D with two different thicknesses. The increasing difference between plane-stress and plane-strain 2D simulations with the increase of hole size suggests non-negligible 3D deformations in resonators with large holes. As expected, the 3D results range from the plane-stress to the plane-strain limits for increasing thicknesses. For a side-to-thickness aspect ratio of 40 (thickness = 10µm) and low fill factors (As1.2 and As2.5) α_{opt} is around 0.1 higher than the one obtained with the plane-stress hypothesis, while for a side-to-thickness aspect ratio of 10 (thickness = 40µm) the 3D TC_f is already quite close to the 2D plane-strain one. While accurate estimates at low α_{opt} cannot be obtained with the model, FEM data show that the compensation method is still working, though at a different (higher) α_{opt}. This is actually an advantage in practical cases, as a higher α gives a better quality factor, as discussed above.

The high p-type doping concentrations are particularly interesting for applications, as they correspond to a doping range where the temperature coefficients of the elastic moduli are saturated (i.e. weakly dependent on doping). This doping window could not be used to fabricate zero-TC_f resonators by doping alone: the full resonators measured in [22] have a TC_f above 2 ppm·K^{-1}. To obtain zero-TC_f full resonators one has to move to a lower doping value, where the doping dependence of the temperature coefficients is higher. However, by adding holes, a zero-TC_f design can be moved to the high p-type doping window. In this case, high accuracy in setting the doping value is not required, as the variance of the TC_f is mostly dependent on the variance of the value of α, which can be controlled more easily. While high values of p-type doping are technologically challenging as they are known to induce high stresses in SOI wafers [41], they have been achieved nonetheless [42].

We also derived an expression (reported in Appendix B) for the second order temperature coefficient $TC2_f$ of perforated resonators, using an approach similar to the one presented in section II for the TC_f. Our model predicts no significant drawback. The two p-type doping, zero-TC_f optimal resonators (first two rows of Table III) have a $TC2_f$ comparable to full resonators at the same doping (Fig. 6), but the full resonators have a first order TC_f of about 2 ppm·K^{-1}. Moreover, the improvement of the $TC2_f$ with increasing p-type doping concentration suggested by data in Fig.6 is a further advantage of moving to the high p-type doping window.

In silicon resonators with very low temperature dependence of the resonance frequency, other possible causes of frequency variability must also be considered. Among these, angular misalignment and spatial fluctuation of dimensions because of etch non-uniformity are among the most prominent. For this reason, we also investigated the robustness of our approach with respect to these effects.

Based on data from [22], [23], the effect of angular misalignment has been simulated over a range of ±2° for the four optimal resonators of Table III. FEM data show that this

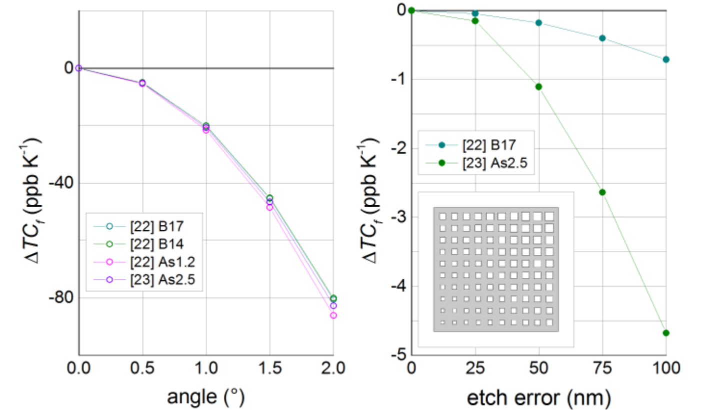

Fig. 7. Variation of the TC_f as consequence of (left) angular misalignment with respect to the SCS crystal for the four optimal resonators, and (right) of a linear dispersion in the dimensions of the holes, schematically represented in the inset, for two optimal resonators.

effect is of the second order with respect to the angle, and alters the TC_f of a few tens of ppb·K^{-1} only in the worst case (Fig. 7, left).

Another possible cause of frequency variation is a dispersion of hole sizes introduced by etch non-uniformity. To evaluate this effect, we designed a worst-case experiment where hole sizes are distributed following a linear function oriented along the resonator diagonal (Fig. 7, right, inset). Specifically, the hole side was incremented or reduced linearly with respect to the nominal optimal values of Table III, so that the maximum error (at the corner holes) is $\pm\varepsilon$, where ε is the etch error in Fig. 7 (right). This distribution replicates a possible non-uniformity in the RIE (Reactive Ion Etching) process typically used to create the holes. We tested an etch error up to 100 nm, again based on data from [22], [23]. The results show that this effect is, to the first order, negligible, and changes the TC_f of a few ppb·K^{-1} only in the worst case. Very similar results were obtained along other directions.

V. Conclusions

In conclusion, we have proposed a new approach to the temperature compensation of MEMS Lamé resonators based on the introduction of a grid of square etch holes. By means of a simple analytical model we showed that the dependence of temperature coefficient of the resonance frequency from the holes size can be ascribed the temperature coefficient of the equivalent material Poisson's ratio. The model was validated with both FEM simulations and experimental data taken from the literature. We also investigated the relation between temperature coefficient and doping in perforated resonators, showing that two regions of the design space allow a first-order temperature compensation of the resonance frequency. This result is extremely interesting from the application point of view, for two reasons. First, because low-temperature coefficient resonators can be designed even with holes, which are often needed in MEMS fabrication. Second and most important, at least one design space region for silicon (the one at high p-doping) is identified that would enable a strong temperature compensation even in the presence of large inaccuracy in the doping concentration.

Appendix A

The simplest way to obtain equations (2b) is to substitute into their right hand sides the expressions of the Young's modulus and Poisson's ratio of a cubic material in terms of its stiffness coefficients. Such expressions can be found in a general form valid in any direction of the crystal in [43] . We report here the special cases of [100] and [110] directions for simplicity:

$$E_{[100]} = C_{11} - \frac{2C_{12}^2}{C_{11}+C_{12}} \quad (8)$$

$$\nu_{[100]} = \frac{C_{12}}{C_{11}+C_{12}} \quad (9)$$

$$E_{[110]} = \frac{4(C_{11}^2+C_{11}C_{12}-2C_{12}^2)C_{44}}{C_{11}^2-2C_{12}^2+C_{11}C_{12}+2C_{11}C_{44}} \quad (10)$$

$$\nu_{[110]} = \frac{C_{11}^2-2C_{12}^2+C_{11}C_{12}-2C_{11}C_{44}}{C_{11}^2-2C_{12}^2+C_{11}C_{12}+2C_{11}C_{44}}. \quad (11)$$

To determine the TC_f of the resonator, TC_{Ep} and $TC_{\nu p}$ are also required. We compute TC_{Ep} and $TC_{\nu p}$ by expanding (8)-(11) in series with respect to the temperature and substituting the values for the C_{ij} and their temperature coefficients from [22], [23]. Using a similar approach, the uncertainties given in the initial data can be propagated, and the errors of these coefficients can be computed as well.

Appendix B

A derivation similar to the one reported in section II for the linear (first order) temperature coefficient TC_f, yields the following expression for $TC2_f$:

$$TC2_f = \frac{1}{2f_{0,eq}}\frac{\partial^2 f_{0,eq}}{\partial T^2} =$$

$$= \frac{1}{2}TC2_L + \frac{1}{2}TC2_{Ep} - \frac{\alpha\nu_p[(\alpha-1)\alpha^k-\alpha]}{2(\alpha-1)[\alpha(\nu_p-1)+1]\alpha^k-2\alpha(\alpha\nu_p+1)}TC2_{\nu p} - \frac{1}{8}TC_L^2 - \frac{1}{8}TC_{Ep}^2 + \frac{3\alpha^2\nu_p^2[\alpha-(\alpha-1)\alpha^k]^2}{8[(\alpha-1)(\alpha(\nu_p-1)+1)\alpha^k-\alpha(\alpha\nu_p+1)]^2}TC_{\nu p}^2 + \frac{1}{4}TC_{Ep}TC_L - \frac{\alpha\nu_p[(\alpha-1)\alpha^k-\alpha]}{4(\alpha-1)[\alpha(\nu_p-1)+1]\alpha^k-4\alpha(\alpha\nu_p+1)}TC_{Ep}TC_{\nu p} - \frac{\alpha\nu_p[(\alpha-1)\alpha^k-\alpha]}{4(\alpha-1)[\alpha(\nu_p-1)+1]\alpha^k-4\alpha(\alpha\nu_p+1)}TC_{\nu p}TC_L \quad (12)$$

where $TC2_x$ denotes the second order temperature coefficient of quantity x. These values can be computed by the same method described in Appendix A for linear coefficients. The value of the second order thermal expansion coefficient $TC2_L$ used in FEM simulations is 8.5 ppb·K^{-2}.

References

[1] J. T. M. van Beek and R. Puers, "A review of MEMS oscillators for frequency reference and timing applications," *Journal of Micromechanics and Microengineering*, vol. 22, no. 1. p. 13001, 2011.

[2] C. T. Nguyen, "MEMS technology for timing and frequency control.," *IEEE transactions on ultrasonics, ferroelectrics, and frequency control*, vol. 54, no. 2. pp. 251–270, 2007.

[3] S. Fanget, S. Hentz, P. Puget, J. Arcamone, M. Matheron, E. Colinet, P. Andreucci, L. Duraffourg, E. Meyers, and M. L. Roukes, "Gas sensors based on gravimetric detection - A review," *Sensors and Actuators, B: Chemical*, vol. 160, no. 1. pp. 804–821, 2011.

[4] H. S. Wasisto, S. Merzsch, A. Waag, E. Uhde, T. Salthammer, and E. Peiner, "Airborne engineered nanoparticle mass sensor based on a silicon resonant cantilever," *Sensors and Actuators, B: Chemical*, 2012.

[5] E. Timurdogan, B. E. Alaca, I. H. Kavakli, and H. Urey, "MEMS biosensor for detection of Hepatitis A and C viruses in serum," *Biosens. Bioelectron.*, vol. 28, no. 1, pp. 189–194, 2011.

[6] A. Heidari, Y.-J. Yoon, M. K. Park, W.-T. Park, and J. M.-L. Tsai, "High sensitive dielectric filled Lamé mode mass sensor," *Sensors Actuators A Phys.*, vol. 188, pp. 82–88, Dec. 2012.

[7] E. Ng, Y. Yang, V. A. Hong, C. H. Ahn, D. B. Heinz, I. Flader, Y. Chen, C. L. M. Everhart, B. Kim, R. Melamud, R. N. Candler, M. A. Hopcroft, J. C. Salvia, S. Yoneoka, A. B. Graham, M. Agarwal, M. W. Messana, K. L. Chen, H. K. Lee, S. Wang, G. Bahl, V. Qu, C. F. Chiang, T. W. Kenny, A. Partridge, M. Lutz, G. Yama, and G. J. O'Brien, "The long path from MEMS resonators to timing products," in *2015 28th IEEE International Conference on Micro Electro Mechanical Systems (MEMS)*, 2015, pp. 1–2.

[8] M. Shahmohammadi, B. P. Harrington, and R. Abdolvand, "Turnover temperature point in extensional-mode highly doped

silicon microresonators," *IEEE Trans. Electron Devices*, vol. 60, no. 3, pp. 1213–1220, 2013.

[9] H. Lee, A. Partridge, and F. Assaderaghi, "Low jitter and temperature stable MEMS oscillators," in *2012 IEEE International Frequency Control Symposium Proceedings*, 2012, pp. 1–5.

[10] A. K. Ismail, J. S. Burdess, A. J. Harris, G. Suarez, N. Keegan, J. A. Spoors, S. C. Chang, C. J. McNeil, and J. Hedley, "The fabrication, characterization and testing of a MEMS circular diaphragm mass sensor," *Journal of Micromechanics and Microengineering*, vol. 18, no. 2. p. 25021, 2008.

[11] J. C. Salvia, R. Melamud, S. A. Chandorkar, S. F. Lord, and T. W. Kenny, "Real-time temperature compensation of mems oscillators using an integrated micro-oven and a phase-locked loop," *J. Microelectromechanical Syst.*, vol. 19, no. 1, pp. 192–201, 2010.

[12] Z. Wu, A. Peczalski, and M. Rais-Zadeh, "Low-power ovenization of fused silica resonators for temperature-stable oscillators," in *2014 IEEE International Frequency Control Symposium (FCS)*, 2014, pp. 1–5.

[13] M.-H. Li, C.-Y. Chen, C.-S. Li, C.-H. Chin, and S.-S. Li, "A Monolithic CMOS-MEMS Oscillator Based on an Ultra-Low-Power Ovenized Micromechanical Resonator," *J. Microelectromechanical Syst.*, vol. 24, no. 2, pp. 360–372, 2015.

[14] Y. Chen, E. J. Ng, Y. Yang, C. H. Ahn, I. Flader, and T. W. Kenny, "In-situ ovenization of Lamé-mode silicon resonators for temperature compensation," in *2015 28th IEEE International Conference on Micro Electro Mechanical Systems (MEMS)*, 2015, pp. 809–812.

[15] K. Sundaresan, G. K. Ho, S. Pourkamali, and F. Ayazi, "Electronically temperature compensated silicon bulk acoustic resonator reference oscillators," *IEEE J. Solid-State Circuits*, vol. 42, no. 6, pp. 1425–1434, 2007.

[16] S. Zaliasl, J. C. Salvia, G. C. Hill, L. W. Chen, K. Joo, R. Palwai, N. Arumugam, M. Phadke, S. Mukherjee, H.-C. Lee, C. Grosjean, P. M. Hagelin, S. Pamarti, T. S. Fiez, K. A. A. Makinwa, A. Partridge, and V. Menon, "A 3 ppm 1.5 x 0.8 mm2 1.0 uA 32.768 kHz MEMS-Based Oscillator," *IEEE J. Solid-State Circuits*, vol. 50, no. 1, pp. 291–302, Jan. 2015.

[17] V. Thakar and M. Rais-Zadeh, "Temperature-compensated piezoelectrically actuated Lamé-mode resonators," in *2014 IEEE 27th International Conference on Micro Electro Mechanical Systems (MEMS)*, 2014, pp. 214–217.

[18] R. Tabrizian, G. Casinovi, and F. Ayazi, "Temperature-stable silicon oxide (SilOx) micromechanical resonators," *IEEE Trans. Electron Devices*, vol. 60, no. 8, pp. 2656–2663, 2013.

[19] W.-T. H. W.-T. Hsu and C. T.-C. Nguyen, "Geometric stress compensation for enhanced thermal stability in micromechanical resonators," *1998 IEEE Ultrason. Symp. Proc. (Cat. No. 98CH36102)*, vol. 1, 1998.

[20] P. A. Hassanpour, P. M. Nieva, and A. Khajepour, "A passive mechanism for thermal stress regulation in micro-machined beam-type structures," *Microsyst. Technol.*, vol. 18, no. 5, pp. 543–556, 2012.

[21] D. R. Myers, R. G. Azevedo, L. Chen, M. Mehregany, and A. P. Pisano, "Passive substrate temperature compensation of doubly anchored double-ended tuning forks," *J. Microelectromechanical Syst.*, vol. 21, no. 6, pp. 1321–1328, 2012.

[22] E. J. Ng, V. A. Hong, Y. Yang, C. H. Ahn, C. L. M. Everhart, and T. W. Kenny, "Temperature Dependence of the Elastic Constants of Doped Silicon," *J. Microelectromechanical Syst.*, vol. PP, no. 99, pp. 1–12, 2014.

[23] A. Jaakkola, M. Prunnila, T. Pensala, J. Dekker, and P. Pekko, "Determination of doping and temperature-dependent elastic constants of degenerately doped silicon from MEMS resonators," *IEEE Trans. Ultrason. Ferroelectr. Freq. Control*, vol. 61, no. 7, pp. 1063–1074, Jul. 2014.

[24] T. Pensala, A. Jaakkola, M. Prunnila, and J. Dekker, "Temperature compensation of silicon MEMS resonators by heavy doping," in *IEEE International Ultrasonics Symposium, IUS*, 2011, pp. 1952–1955.

[25] A. Hajjam, A. Logan, and S. Pourkamali, "Doping-induced temperature compensation of thermally actuated high-frequency silicon micromechanical resonators," *J. Microelectromechanical Syst.*, vol. 21, no. 3, pp. 681–687, 2012.

[26] R. W. Keyes, "Electronic Effects in the Elastic Properties of Semiconductors," in *Solid State Physics Volume 20*, 1968, pp. 37–90.

[27] A. Gualdino, J. Gaspar, V. Chu, and J. P. Conde, "Sub-micron gap in-plane micromechanical resonators based on low-temperature amorphous silicon thin-films on glass substrates," *J. Micromech. Microeng.*, vol. 25, no. 7, p. 75026, Jul. 2015.

[28] H. Zhu, Y. Xu, and J. E.-Y. Lee, "Piezoresistive Readout Mechanically Coupled Lamé Mode SOI Resonator With Q of a Million," *J. Microelectromechanical Syst.*, vol. 24, no. 4, pp. 771–780, Aug. 2015.

[29] S. A. Chandorkar, R. N. Candler, A. Duwel, R. Melamud, M. Agarwal, K. E. Goodson, and T. W. Kenny, "Multimode thermoelastic dissipation," *J. Appl. Phys.*, vol. 105, no. 4, p. 43505, 2009.

[30] L. Luschi and F. Pieri, "Periodically Structured Lamé Resonators as High Sensitivity Resonant Mass Sensors," *Procedia Eng.*, vol. 87, pp. 228–231, 2014.

[31] X. Rottenberg, R. Jansen, V. Cherman, A. Witvrouw, H. A. C. Tilmans, M. Zanaty, A. Khaled, and M. Abbas, "Meta-materials approach to sensitivity enhancement of MEMS BAW resonant sensors," in *IEEE SENSORS 2013 - Proceedings*, 2013, pp. 1–4.

[32] L. Luschi and F. Pieri, "An analytical model for the resonance frequency of square perforated Lamé-mode resonators," *Sens. Actuators B*, vol. 222, pp. 1233–1239, Jan. 2016.

[33] A.-J. Wang and D. L. McDowell, "In-Plane Stiffness and Yield Strength of Periodic Metal Honeycombs," *Journal of Engineering Materials and Technology*, vol. 126, no. 2. p. 137, 2004.

[34] C. Bourgeois, E. Steinsland, N. Blanc, and N. F. de Rooij, "Design of resonators for the determination of the temperature coefficients of elastic constants of monocrystalline silicon," in *Proceedings of International Frequency Control Symposium*, pp. 791–799.

[35] L. J. J. Walpole, "The elastic shear moduli of a cubic crystal," *J. Phys. D. Appl. Phys.*, vol. 19, no. 3, pp. 457–462, Mar. 1986.

[36] E. J. Ng, "private communication." 2014.

[37] C. Tu and J. E.-Y. Lee, "Thermoelastic Dissipation in Etch-Hole Filled Lamé; Bulk-Mode Silicon Microresonators," *IEEE Electron Device Lett.*, vol. 33, no. 3, pp. 450–452, Mar. 2012.

[38] L. Shao and M. Palaniapan, "Effect of etch holes on quality factor of bulk-mode micromechanical resonators," *Electron. Lett.*, vol. 44, no. 15, p. 938, 2008.

[39] R. Tabrizian and F. Ayazi, "Thermo-acoustic engineering of silicon microresonators via evanescent waves," *Appl. Phys. Lett.*, vol. 106, no. 26, p. 263504, Jun. 2015.

[40] J. J. Hall, "Electronic Effects in the Elastic Constants of n-Type Silicon," *Phys. Rev.*, vol. 161, no. 3, pp. 756–761, Sep. 1967.

[41] P. Sievilä, J. Mäkinen, M. Tilli, and I. Tittonen, "Dopant-induced stress in microfabricated silicon devices," *J. Appl. Phys.*, vol. 114, no. 4, p. 43512, 2013.

[42] E. J. Ng, Y. Yang, Y. Chen, and T. W. Kenny, "an Etch Hole-Free Process for Temperature-Compensated , High Q , Encapsulated Resonators," in *Solid-State Sensors, Actuators and Microsystems Workshop*, 2014, pp. 99–100.

[43] M. A. Hopcroft, W. D. Nix, and T. W. Kenny, "What is the Young's Modulus of Silicon?," *J. Microelectromechanical Syst.*, vol. 19, no. 2, pp. 229–238, Apr. 2010.